Shock Waves in Outflows from Young Stars

Patrick Hartigan
Dept. of Physics and Astronomy, Rice University, Houston TX USA

November 1, 2002

Abstract. This review focuses on physics of the cooling zones behind radiative shocks and the emission line diagnostics that can be used to infer physical conditions and mass loss rates in jets from young stars. Spatial separations of the cooling zones from the shock fronts, now resolvable with HST, and recent evidence for C-shocks have greatly increased our understanding of how shocks in outflows interact with the surrounding medium and with other material within the flow. By combining multiple epoch HST images, one can create 'movies' of flows like those produced from numerical codes, and learn what kinds of instabilities develop within these systems.

Keywords: shock waves, mass loss rates, stellar jets

1. Introduction

Emission lines from Herbig-Haro objects have been known to arise from the cooling regions behind shock waves for some time (e.g. Schwartz, 1983). These shocks form as material emerges from a collimated jet and interacts with previously ejected gas and with the surrounding medium. The shock speeds are low enough and the densities high enough that the shocked gas cools by radiating emission lines, a type of shock known as a radiative shock. The line emission is extremely useful because it constrains the temperatures, densities, ionization fractions, and kinematics in jets.

To use the observations to their fullest one must understand the physics of radiative shocks under conditions appropriate for HH flows. Many reviews of shock physics and HH objects exist throughout the literature, so this paper will focus on specific topics of current interest, such as mass loss rates, precursors, magnetic fields, and motions. An excellent review of astrophysical shocks is given by Draine & McKee (1993), and a thorough summary of HH history and current research has just been compiled by Reipurth & Bally (2001). In addition, Hartigan et al. (2000a) summarize how shocks can be used to understand HH flows, and Eislöffel et al. (2000) review the status of observations of these systems.

2. Physics of Radiative Shocks

2.1. Jump Conditions

The most familiar type of shock (a so-called 'J' or jump-shock) is one where the flow variables undergo a discontinuous change at some interface, and the entropy of the fluid increases as material flows through the interface. The preshock and postshock material are each characterized by (i) a gas pressure P, (ii) temperature T, (iii) magnetic field B, (iv) density n, and (v) velocity V with respect to the shock. These ten variables are related to one other by equations of state in the (i) preshock and (ii) postshock material, conservation of (iii) mass, (iv) momentum, and (v) energy across the shock, and (vi) a requirement that the fluid is tied to field lines. Four more equations are needed to solve the system, and these are specified by the preshock velocity, density, magnetic field, and temperature (equivalently the Mach number $\mathrm{M} = \mathrm{V}/\mathrm{C}_S$, where $\mathrm{C}_S^2 = \gamma \mathrm{kT/m}$ is the sound speed, γ the ratio of specific heats, and m is the average mass of the incident atoms).

In the non-magnetic case, if the subscripts 1 and 2 refer to the preshock and postshock gas, respectively, then the energy, momentum, and mass equations can be combined to a quadratic equation for the compression factor C across the shock, whose solution is (e.g. Draine & McKee, 1993)

$$C = \frac{n_2}{n_1} = \frac{v_1}{v_2} = \frac{\gamma + 1}{(\gamma - 1) + 2/M^2} \tag{1}$$

The postshock temperature is then

$$T_2 = \frac{2(\gamma - 1) m v_1^2}{(\gamma + 1)^2 k} \tag{2}$$

In the limit of high Mach number and $\gamma = 5/3$,

$$C \rightarrow \ 4 \text{ and } T_2 \ \rightarrow \frac{3 m v_1^2}{16 k} = 1.38 \times 10^5 \left(\frac{v_1}{100 \text{ km s}^{-1}} \right)^2 \ ^\circ\mathrm{K} \tag{3}$$

for a solar composition ($\mu = 0.61$). For nonmagnetic oblique shocks, the component of motion along the interface is conserved across the shock, so the shock velocity is simply the component of the velocity normal to the shock.

The magnetic case is considerably more complicated, and the solutions depend upon the angle of the field relative to surface of the shock (see Draine & McKee, 1993). For the case where the component of the

field perpendicular to the shock is zero, equation (1) becomes a cubic, but can be factored to

$$(C-1)\left[\left(\frac{2-\gamma}{M_A^2}\right)C^2 + DC - (\gamma+1)\right] = 0 \tag{4}$$

where M_A is the Alvenic Mach number = V/V_A with V_A the Alven speed, and

$$D = \gamma - 1 + \frac{2}{M^2} + \frac{\gamma}{M_A^2} \tag{5}$$

The solution of equations (4) and (5) is

$$C = \frac{2\,(\gamma+1)}{D + \left[D^2 + 4(\gamma+1)(2-\gamma)M_A^{-2}\right]^{0.5}} \tag{6}$$

which reduces to equation (1) in the limit of small magnetic fields ($M_A \rightarrow \infty$). If one redefines the Mach number in terms of the fast magnetosonic speed $V_F = (C_S^2 + V_A^2)^{0.5}$, then C depends on the Mach number in a similar way to the nonmagnetic case (Fig. 1).

2.2. Cooling

The equations in the previous section only solve for conditions immediately behind the shock front. Further downstream the gas typically becomes denser as it cools and radiates emission lines. However, if the density in the shocked gas is low enough or the gas is so hot that most abundant elements are stripped of outer electrons, the radiative cooling time can become longer than the age of the shock, or the gas may cool by expansion rather than by radiation. When no radiation is visible from cooling zones the shock is called 'nonradiative'. When radiative cooling does occur, emission lines from a given ion originate from a specific zone where that ion exists. The postshock gas is not in ionization equilibrium; initially the gas is much less ionized than its temperature would indicate, and as the gas cools it can be reheated by photons from the hotter portion of the shock, which leads to a higher ionization than would otherwise be expected at the lower temperatures (Raymond, 1979).

The cooling rate L (erg s^{-1}) enters into the equation for the rate of change of the enthalpy h per nucleus (Cox, 1972):

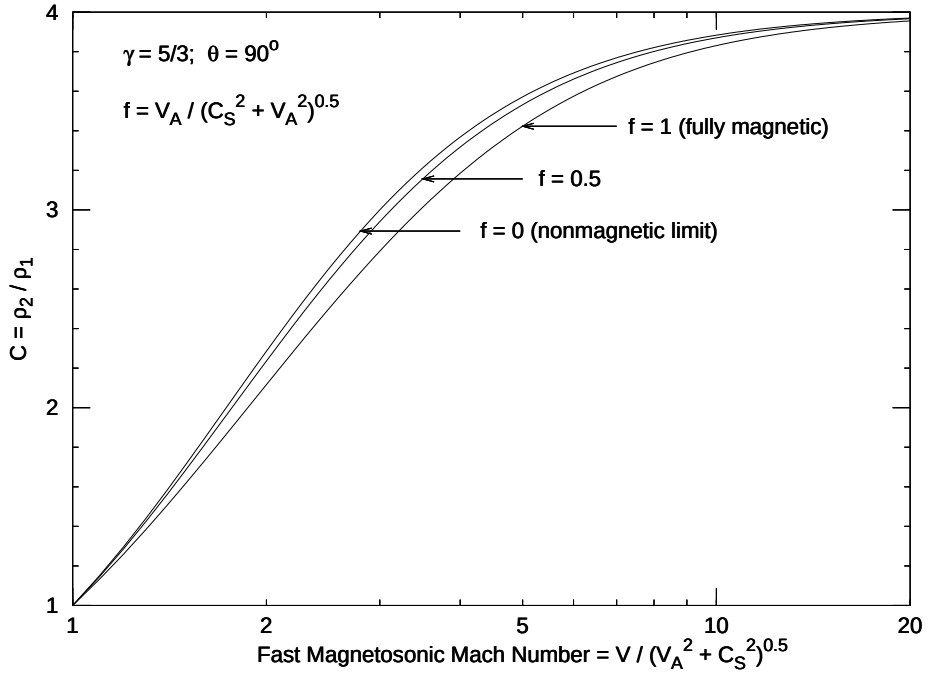

Figure 1. Compression across a magnetic shock as a function of the fast magnetosonic Mach number for an ideal monoatomic gas when the incident magnetic field lies entirely in the plane of the shock ($\theta = 90°$). The f = 0 line corresponds to the nonmagnetic case (equation 1). When the shock velocity greatly exceeds both V_A and C_S, the compression approaches 4, while C $\rightarrow$ 1 for the weakest shocks.

$$\frac{dh}{dt} = L; \quad h = \frac{mv^2}{2} + E_I + \frac{5}{2}\frac{(n+n_e)kT}{n} + \frac{B^2}{4\pi n} \tag{7}$$

where E_I and m are the mean ionization energy and mass per particle, respectively. As the gas cools, progressively lower ionization states are reached. For example, a high velocity shock may have lines of [O III] near the front, followed by lines of [O II] and finally [O I] (e.g. Dopita, 1976). All the important atomic processes, such as charge exchange, photoionization, recombination, collisional excitation and deexcitation, and collisional ionization are included in all modern shock models.

The magnetic field plays a very important role in the postshock flow, even if the magnetic pressure is negligible compared to the ram pressure at the shock front. Because B $\sim$ n and the gas pressure P $\sim$ nT $\sim$ constant in the cooling zone of a weakly magnetized shock, B $\sim$ T^{-1} as long as the magnetic pressure is negligible. Hence, the ratio of magnetic to thermal pressures scales as T^{-2}. The temperature can easily drop by 2 orders of magnitude as the gas cools (equation 2),

so the magnetic pressure typically becomes comparable to the thermal pressure as the postshock gas cools. The main dynamical effect of the increased magnetic pressure is to inhibit the compression within the cooling zone (e.g. Hartigan et al., 1994).

When the shock velocity exceeds $\sim$ 140 $\mathrm{km\,s^{-1}}$, thermal instabilities may occur in the hot postshock gas (Innes et al., 1987). Recent numerical simulations of this phenomenon by Sutherland (2002) show that these high velocity shocks develop a fractal-like structure in their cooling zones. The effect of this instability on HH jets is unclear; most HH shocks lie below the instability velocity, and those that exceed it are always bow shocks of some sort, where only the apex of the bow should be unstable. Magnetic fields may also inhibit the instability (Innes, 1992).

2.3. Balmer Emission and the Shock Front

Although nonradiative shocks lack cooling zones, emission lines can occur when gas becomes heated immediately behind these shocks (Chevalier & Raymond, 1978; Chevalier et al., 1980). For example, any neutral hydrogen that enters the shock may be excited collisionally and radiate Balmer line emission before the atom is ionized. Because the cross sections for collisional excitation and ionization mirror each other across a wide energy range (Hartigan et al., 2000a), the number of Balmer photons per incident H atom is relatively independent of shock velocity. Hence, Balmer emission at the front should exist over a wide range of shock velocities. As long as neutral H is present ahead of the shock, a collisional component to the H line profiles exists even if the postshock gas does not cool radiatively.

In supernovae remnants, Balmer filaments often mark the leading edge of the blast wave (e.g Smith et al., 1991), and charge exchange gives rise to a broad component and a narrow component to the emission line profiles (Chevalier & Raymond, 1978). The ratio of these components depends on the ratio of ion and electron temperatures (Ghavamian et al., 2001), and both the shock velocity and inclination of the shock plane to the observer are derivable from the line profile shapes. Broad and narrow component line profiles have not yet been observed in HH shocks, but Balmer emission from collisions at the shocks has, and provides an effective means to study these systems.

2.4. Radiative Precursors

Precursors refer to heating that occurs ahead of the main shock front. Examples include radiative precursors, where ultraviolet photons from the postshock gas travel upstream and ionize the preshock gas (Shull &

McKee, 1979). For very high shock velocities and densities, radiation from this precursor can dominate the total line emission (Dopita & Sutherland, 1996), but radiative precursors should not produce significant fluxes in young stellar jets. However, the ionization state of the preshock gas does affect the postshock conditions in HH objects; the postshock temperature is lower if the preshock gas is neutral than if the gas is ionized because part of the kinetic energy in the neutral case goes into ionization (Cox & Raymond, 1985). In bow shocks like those in HH jets, the preshock ionization should be highest at the apex of the bow, though a full time-dependent simulation is needed to solve this problem (e.g. Raymond et al., 1988).

2.5. Magnetic Precursors

If magnetic fields are present, the ions and neutrals need to be considered as separate fluids in the equations (Draine, 1980; Draine et al., 1983). When the shock speed is supersonic but submagnetosonic, magnetic waves push ions through the neutrals in the preshock gas. As a result, friction between ions and neutrals generates a warm precursor ahead of the shock. This precursor can become strong enough that it overwhelms the J-shock defined in §2.1 and produces a smooth rise in the density and temperature known as a C-shock. Both J-shocks and C-shocks are included in the expanded definition of a shock front given by Draine (1980) as an irreversible pressure-driven disturbance.

3. Application to Young Stellar Objects

3.1. Shock Waves in Stellar Jets

Stellar jets typically appear as a series of highly collimated knots, followed at various places along the flow with larger bow-shaped structures. When the flow has a large neutral component, sharp Hα features identify locations of shocks in the flow (see §2.3). As predicted by theory and by numerical simulations (e.g. Lind, 1989), a shock about the size of the jet often lies along the axis of the flow inside the large bow shocks. Known as the Mach disk, this shock marks where the jet decelerates as it encounters the bow shock. Mach disks do not occur if the bow moves faster than the jet (as might happen if the flow velocity decreases with time). Several fine examples of bow shock/Mach disk pairs now exist (Morse et al., 1992; Heathcote et al., 1996).

When observed with the excellent spatial resolution of HST, jets from young stars usually break up into a series of nested bow shocks (Reipurth et al., 1997). Each bow shock moves into the wake of a

previous ejection, which is why proper motions in jets can be several hundred km s^{-1} even though the shock velocities are only ~ 40 km s^{-1}. The wakes of these bow shocks are visible well away from the axis of the jet, but they fade sharply away from the jet. Hence, the density exterior to the jet is at least an order of magnitude lower than it is within the jet, and plays no role in collimating the flows. This result is not surprising in light of the classic images of HH 30 (Burrows et al., 1996), which clearly show the jet to be collimated within tens of AU from the star, well inside the curved structure of the flared accretion disk.

Unlike extragalactic jets, where hot gas billows away from the bow shocks and may even flow backwards and interact with the jet, in stellar jets the gas that flows through the Mach disk and bow shock cools, and thus stays within the vicinity of the bow. The result is a series of shells that move outward and sometimes interact with one another to create more shocks.

3.2. Magnetic fields

Most theoretical models of jet collimation use magnetic fields from accretion disks. Unfortunately, magnetic fields are difficult to measure in jets because the line ratios from magnetic shocks resemble those from nonmagnetic shocks with lower shock velocities (Hartigan et al., 1994). The component of the field parallel to the shock front affects the compression in the cooling zone (see §2.2). Using this effect, Morse et al. (1992) found B ~ 30 μG in the preshock gas of HH 34. Line ratios also limit field strengths in the HH 111 jet (Hartigan et al., 2001). For reference, if we equate the magnetic and thermal pressures in a typical cooling zone of a radiative shock with T$\sim 10^4$ K and n $\sim 10^4$ cm^{-3}, we find B ~ 600 μG. A milli-Gauss field is too small to redirect the jet significantly, but does affect the compression markedly.

The only other estimate of HH object magnetic fields in the literature seems to be that of Ray et al. (1997), who infer large fields of several Gauss from measurements of polarized radio emission of T TauS that they attribute to an HH knot ~ 10 AU from the star. If confirmed, magnetic fields will dominate the dynamics within these objects.

3.3. Molecular Emission and C-shocks

Several of the most spectacular jets (e.g. HH 212 Zinnecker et al., 1998) radiate molecular lines that most likely arise in C-shocks (e.g. Davis et al., 1999). C-shocks and magnetic precursors also mark the locations where jets deposit energy and momentum into molecular outflows. For example, in the massive molecular outflow Cepheus A, H_2 lies outside

of Hα, as expected for a precursor. Remarkably, [S II] lies between H_2 and Hα, indicating that it, too, comes from the precursor (Hartigan et al., 2000b). The physical size of the precursor is in line with that predicted by theory. The mechanism of ion-neutral heating in the C-shock is very difficult to model accurately, and this is one area of HH research where both observations and theory have room to improve. Kinematics of C-shocks are discussed by Flower et al. elsewhere in this issue.

4. Mass Loss Rates

The ratio of mass outflow rates to mass accretion rates is a key observable that is also predicted by models of jets driven by accretion disks. Mass loss rates are crucial for understanding how jets are collimated and driven, and also determine the impact these flows have on the ambient molecular cloud. The following summarizes the strengths and weaknesses of the most commonly used methods for estimating this important number.

4.1. Hollenbach's Method

One of the simplest methods to measure mass loss rates was first described by Hollenbach (1985). In radiative shocks, the [O I] 63μm line dominates the cooling once the temperature drops below about $T_o \sim 5000$K. Hence, each atom that passes through the shock radiates approximately $(3/2)kT_o$ of energy in this line. The mass loss rate is then proportional to the luminosity L_{63} in the 63μm line

$$\dot{M} = \frac{2L_{63}}{3kT_o\mu m_H} \tag{8}$$

The main advantages of this method are that it can be used whenever the luminosity in the [O I] 63μm line is known, and because the line is in the far-infrared, reddening corrections are unimportant. The principal disadvantage is that it assumes that each atom goes through only a single shock, and as such provides only an upper limit to the mass loss for flows like stellar jets that have many shocks. The large beam size associated with far-IR observations and the relatively poor instrumental sensitivity also confuse the interpretation and limit the number of objects where this method can be applied.

4.2. [O I] λ6300 Luminosity

A variant of Hollenbach's method has been used by Kwan & Tademaru (1995) for the [O I] 6300Å transition. The method is the same, except equation 8 must be corrected by a factor f that represents the number of [O I] 6300Å photons emitted per atom incident to the shock, and the mass loss rate is increased by a factor V/V_S where V is the flow speed and V_S is the shock velocity in the jet. The factor f can be found from shock models and the ratio V/V_S is known reasonably well from proper motion studies and emission line ratios.

When applied to T Tauri stars, where there is typically both a low velocity component that may arise from the disk and a high velocity component in the jet, it is better to use only the high velocity component for the line luminosity. Hartigan et al. (1995) used the high-velocity luminosity within an aperture to infer a mass; the velocity and aperture size then give a mass loss rate. Unlike the KT and Hollenbach methods, this procedure will give the same mass loss rate if a larger aperture is used to observe a radiating jet. However, in converting from luminosity to mass one must assume a characteristic density, which is only known to a factor of ~ 4 because of uncertainties about the appropriate average density of the flow (§4.3). Reddening corrections affect these two methods and other procedures that use optical line luminosities to estimate mass loss rates.

4.3. Emission Line Ratios from Shocks

By using all the emission lines present in the spectrum and constructing a shock model that fits them, one can solve for the preshock density and the shock velocity (Hartigan et al., 1994). The mass loss rate is simply nmVA, where n is the density, m the average mass per particle, V the bulk velocity of the flow, and A the cross-sectional area of the jet. The tricky part to estimate is $n = n_e X^{-1}$, where n_e is the electron density and X is the ionization fraction. The electron density comes from the ratio of the red lines of [S II], and the ionization fraction from the shock model, weighted according to where [S II] emits.

A drawback with this procedure is that it is rather involved; finding the best match to the fluxes of dozens of emission lines can be a lengthy procedure. Probably the most serious problem is that jets are inherently clumpy. Mass loss rates in the postshock gas always exceed those in the preshock gas because the postshock gas is denser. Emission lines come entirely from the postshock gas, so some sort of average of the preshock and postshock regions are appropriate for an average mass loss rate.

4.4. The BE Method

Bacciotti et al. (1995) suggested a way to measure ionization fractions in jets based on ratios that involve only the brightest lines in stellar jets – Hα, [S II], [O I] and [N II] – that are relatively easy to observe in most cases. The procedure approximates the line emitting region as arising from a single temperature, density, and ionization fraction. However, in the cooling zone of a radiative shock, where more highly ionized species emit, on average, closer to the shock than do more neutral atoms, each emission line comes from a range of densities and temperatures throughout the cooling zone. Serious problems occur when this method is applied to Hα, which has a strong collisional component whenever the preshock gas is neutral; any ratios that involve Hα must take these nonequilibrium processes into account.

Fortunately, Hα is not essential to this idea; charge exchange ties the ionization of O, and, to a lesser degree N, to that of H. Hence, the line ratio of O I/N II is sensitive to the ionization fraction (Bacciotti & Eislöffel, 1999; Bacciotti, 2002). However, if the cooling zone is not well-resolved spatially between the different forbidden lines (a more difficult task than separating the forbidden line regions from the Balmer emission at the shock), then the [S II] ratio, which determines the electron density, is measured in a location where the physical conditions differ from those where one measures [N II] and [O I]. The question arises as to how well this method works in practice, given that it uses such a simple model for the cooling zone.

Tests of the above (BE) method, applied point by point within the cooling zone of a 35 $\mathrm{km\,s^{-1}}$ and a 70 $\mathrm{km\,s^{-1}}$ radiative shock by the author show that the method in fact follows the ionization fraction quite well except near the shock front. Tests on stellar jets (Table 1) also show good agreement. It is still uncertain over what range of parameters the BE method might operate. It will likely fail when the shock velocity exceeds $\sim$ 100 $\mathrm{km\,s^{-1}}$ and photoionization becomes important in the cooling zones. Higher shock velocities also introduce more ionization states for each element, which are not included in the method.

The advantage of the BE method is that it is simple, and the emission lines it requires are bright in stellar jets. As described above, the method will not work in all cases, but it may prove quite useful for many HH flows. One disadvantage is that the method uses only a few of the bright lines; other line ratios may give different answers. As with the other methods discussed so far, the main drawback with BE may be clumpy flows – any cold preshock gas that does not emit line radiation, but still partakes of the flow, is ignored by this method.

	X(HMR94)	X(BE99)
HH 34	0.026	0.027
HH 47	0.055	0.070
HH 111	0.052	0.064

Table 1 The ionization fraction of three jets from shock models (2nd column, Hartigan et al., 1994), and BE (3rd column, Bacciotti & Eislöffel, 1999).

4.5. Irradiated Jets

All of the above methods give a mass loss rate of zero if no shocks occur in the outflow. Ideally, we would like to measure all of the mass in the jet, not just the part that is heated by shocks. Nature provides a convenient means to do this if the jet lies within an H II region such as Orion (Bally & Reipurth, 2001). Heating within irradiated jets is a combination of shocks and photoionization, so interpreting the line emission will not be easy, but at least in these cases we can be confident we observe all of the gas in the jet. The discovery of irradiated jets is still rather new, and models of the line emission do not yet exist. However, external photoionizing sources are input parameters to modern shock codes, so the problem can be solved with existing tools.

5. Movies of Stellar Jets from HST

By combining HST images of jets taken at different times it is possible to discern the types of motions present. Two epochs have so far been observed for four bright jets, and interpolations between these epochs make it possible to follow the structural changes more easily than by blinking. The main results of these studies for HH 111 (Hartigan et al., 2001), HH 34 (Reipurth et al., 2002), and HH 1 (Bally et al., 2002) have already been published. The interpolation method, and a brief description of the HH 47 results is in press (Hartigan, 2003), with a more detailed description of HH 47 in preparation (Heathcote et al., 2003).

Readers of this article are encouraged to download the movies located at http://sparky.rice.edu/~hartigan/movies.html. Space limits the discussion of the movies in this review, but the main result is that although jets appear to have a very complex structure, that structure to first order moves together as a unit. The most interesting regions dynamically are the bow shocks and Mach disks, where the flow appears very clumpy both along the jet and perpendicular to it. Shear occurs along the edges of the bows, and several new knots appear between the four years that separate the epochs.

References

Bally, J., & Reipurth, B. 2001, ApJ 546, 299
Bally, J., Heathcote, S., Reipurth, B., Morse, J., Hartigan, P., & Schwartz, R. D. 2002, AJ 123, 2627
Bacciotti, F. 2002, RMAA Serie de Conferencias 13, 8.
Bacciotti, F., Chiuderi, C., & Oliva, E. 1995, A&A 296, 185
Bacciotti, F., & Eislöffel, J. 1999, A&A 342, 717
Burrows, A. et al. 1996, ApJ 473, 437
Chevalier, R. A., & Raymond, J. C. 1978, ApJ 225, L27
Chevalier, R. A., Kirshner, R., & Raymond, J. 1980, ApJ 235, 186
Cox, D. P. 1972, ApJ 178, 143
Cox, D. P., & Raymond, J. 1985, ApJ 298, 651
Davis, C. J., Smith, M. D., Eislöffel, J., & Davies, J. K. 1999, MNRAS 308, 539.
Dopita, M. A. 1976, ApJ 209, 395
Dopita, M. A., & Sutherland, R. 1996, ApJS 102, 161
Draine, B. T. 1980, ApJ 241, 1021
Draine, B. T., Roberge, W. G., & Dalgarno, A. 1983, ApJ 264, 485
Draine, B. T. & McKee, C. F. 1993, ARA&A 31, 373
Eislöffel, J., Mundt, R., Ray, T. P., & Rodriguez, L. F. 2000, in "Protostars and Planets IV", V. Mannings, A. P. Boss & S. S. Russell eds., (Tucson: U of A Press), 815
Ghavamian, P., Raymond, J., Smith, R. C., & Hartigan, P. 2001, ApJ 547, 995
Hartigan, P., Bally, J., Reipurth, B., & Morse, J. 2000a, in "Protostars and Planets IV", V. Mannings, A. P. Boss & S. S. Russell eds., (Tucson: U of A Press), 841
Hartigan, P., Edwards, S., & Ghandour, L. 1995, ApJ 452, 736
Hartigan, P., Morse, J., & Bally, J. 2000b, AJ 120, 1436
Hartigan, P., Morse, J., Reipurth, B., Heathcote, S. & Bally, J. 2001, ApJ 559, L157
Hartigan, P. 2003, RMA&A Serie de Conferencias, in press
Hartigan, P., Morse, J., & Raymond, J. 1994, ApJ 436, 125
Heathcote, S. et al. 2003, in preparation
Heathcote, S., Morse, J., Hartigan, P., Reipurth, B., Schwartz, R.D., Bally, J., & Stone, J. 1996, AJ 112, 1141
Hollenbach, D. 1985, Icarus 61, 36
Innes, D. E. 1992, A&A 256, 660
Innes, D. E., Giddings, J. R., & Falle, S. A. E. G. 1987, MNRAS 226, 67
Kwan, J. & Tademaru, E. 1995, ApJ 454, 382
Lind, K., Payne, D., Meier, D., Blandford, R. D. 1989, ApJ 344, 89
Morse, J., Hartigan, P., Cecil, G., Raymond, J., & Heathcote, S. 1992, ApJ 399, 231
Ray, T., Muxlow, T. W. B., Axon, D. J., Brown, A., Corcoran, D., Dyson, J., & Mundt, R. 1997, Nature 385, 415
Raymond, J. 1979, ApJS 39, 1
Raymond, J., Hartmann, L., & Hartigan, P. 1988, ApJ 326, 323
Reipurth, B., Hartigan, P., Heathcote, S., Morse, J. & Bally, J. 1997, AJ 114, 757
Reipurth, B. & Bally, J. 2001, ARA&A 39, 403
Reipurth, B., Heathcote, S., Morse, J., Hartigan, P., & Bally, J. 2002, AJ 123, 362
Schwartz, R. D. 1983, ARA&A 21, 209
Shull, J. M., & McKee, C. F. 1979, ApJ 227, 131
Sutherland, R. 2002, in preparation.
Smith, R. C., Kirshner, R. P., Blair, W. P., & Winkler, P. 1991, ApJ 375, 652
Zinnecker, H., McCaughrean, M., & Rayner, J. 1998, Nature 394, 862